JOURNAL OF MATERIALS SCIENCE 28 (1993) 5765–5769

Impedance analyses of cooling-rate effects on the depletion layer of PTCR materials

CHANG-JUNG KIM, KWANGSOO NO
Department of Ceramic Science and Engineering, Korea Advanced Institute of Science and Technology, Deajon, Korea

Cooling-rate effects on the depletion layer of $BaTiO_3$ positive temperature coefficient of resistance (PTCR) were analysed using d.c. resistivity and a.c. complex impedance spectroscopy. As the cooling rates decreased, the d.c. resistivity of the sample increased. A.c. complex impedance spectra showed that the observed d.c. resistivity increase was mainly due to the grain-boundary resistivity increase. The grain resistivity also exhibited relatively weak PTCR behaviour. The built-in potential and the depletion-layer width were analysed using the a.c. complex impedance data. Slow cooling rate produced higher built-in potential and large depletion-layer width. The relationship between the built-in potential and the depletion-layer width at different temperatures was analysed and used to explain the observed grain-boundary resistivity change. The resistivity decrease in the low-temperature region was due to the depletion-layer width decrease. The resistivity jump over the temperature was due to both the built-in potential and the depletion-layer width changes.

1. Introduction

Positive temperature coefficient of resistance (PTCR) materials were originally developed in early 1950s. The PTCR effect in doped barium titanate ceramics is characterized by a large and rapid non-linear increase in electrical resistance as the temperature increased over the ferroelectric transition temperature [1].

Various attempts have been made to explain the PTCR effect [2–4], and it is usually assumed that the grain boundaries are responsible [5–9], because single crystals do not show the effect [10]. From those studies, Heywang's model was proposed to explain the electronic structure of the grain boundary [2]. This model treats the grain boundary as a n-type Schottky barrier or a depletion layer, which eliminates conduction electrons from the boundary [3, 5, 11]. This barrier produces a high resistivity state above the ferroelectric transition temperature. Below the transition temperature, the potential barrier is diminished because the surface states are wholly or partly compensated by a high dielectric constant and spontaneous polarization. From the investigation of Daniels and Wernicke [12], the cooling rate affects the depletion-layer width at the grain boundary: the slower the cooling rate, the wider this layer becomes. Therefore, the resistivity of the sample becomes higher at the transition temperature.

According to the depletion-layer model, the resistivity of the grain-boundary layer of unit area can be defined as

$$\rho = \rho_0 \exp(eV_{bi}/kT) \quad (1)$$

where ρ_0 is a constant, e is the electron charge, V_{bi} is the built-in potential barrier height at the grain boundary, k is the Boltzmann constant and T is the absolute temperature.

From the Schottky barrier model [13], the depletion layer width, W, and the capacitance, C, per depletion layer per unit area are defined as

$$W = [2C(V_{bi} - kT/e)/eN_D]^{1/2} \quad (2)$$

and

$$C = [e\varepsilon_0\varepsilon_r N_D/2(V_{bi} - kT/e)]^{1/2} \quad (3)$$

where N_D is the donor impurity density, and ε_0 and ε_r are the vacuum permittivity and the relative dielectric constant, respectively, of the depletion layer. Because V_{bi} is inversely proportional to the dielectric constant, ε_r, which is varied sharply near the transition temperature, V_{bi} is also a function of temperature, and so we may not direct the value of V_{bi} at different temperatures from Equation 1. The combination of Equations 1 and 3 gives the values of V_{bi} at different temperatures [14]. A donor impurity density, N_D, can be calculated from the doping concentration, and is a constant at different temperatures. The depletion-layer width, W, may be calculated using Equation 2.

A.c. impedance spectroscopy has been widely used to distinguish between the grain resistance and grain-boundary resistance [15–17]. The plot of the real part of the total impedance versus the imaginary part as a parametric function of frequency shows a distinctive feature characterizing a specific combination of the circuit elements.

In this paper, a.c. impedance spectroscopy was used to separate the grain-boundary resistivity and the grain-boundary capacitance from the bulk components. In this way, the relationships between the cooling

0022–2461

rate and the grain resistivity, the barrier height and the depletion-layer width, and between the depletion-layer width and the barrier height at different temperatures, were shown.

2. Experimental procedure

A common powder-mixing technique was used for preparing n-type doped $BaTiO_3$ specimens. The doping concentration of Sb_2O_3 was 0.1 mol %. 0.2 mol % excess TiO_2 and 0.4 mol % SiO_2 were added for control of stoichiometry and decreasing sintering temperature, respectively. $BaTiO_3$, Sb_2O_3, TiO_2, and SiO_2 powders were mixed with an organic binder in a polyethylene jar using distilled water and ZrO_2 balls for 24 h. The powder mixture was then dried. Pellets approximately 2 mm thick were pressed from the dried powder mixture in a 15 mm diameter steel mould at 570 kg cm^{-2} pressure. The pellets were then sintered at 1330 °C for 1 h. The samples were heated at 150 °C h^{-1} to 600 °C, the temperature was held at 600 °C for 2 h in order to burn out the organic binder, and the temperature was increased at 300 °C h^{-1} to 1330 °C. After soaking for 1 h, the samples were cooled at different rates: 6, 12, 25, 50, and 100 °C h^{-1}, down to 1000 °C in order to provide different grain-boundary electronic structures. Below 1000 °C, the samples were cooled at furnace rate to room temperature.

Both flat surfaces of the specimens were rubbed with indium–gallium alloy as electrode. The d.c. resistances and the a.c. complex impedance of the specimens were measured during heat-up in a computer-controlled measuring system consisting of Fluke 8502A digital multimeter, HP4192A impedance analyser, and a furnace designed specially for minimizing the possible stray capacitance and inductance effects between the lead wires and the heating elements. The grain-boundary resistances, the grain-boundary capacitances, and the bulk resistances of the specimens at each temperature were calculated using the a.c. complex impedance data and a circuit model. The a.c. frequency range used in this study was from 5 Hz to 13 MHz. The grain sizes of the specimens were measured using an optical microscope. The polished surfaces of the specimens were etched using an etching solution: several drops of 48% HF in 100 ml 5% HCl [18].

3. Results and discussion

Fig. 1 shows the resistivity versus temperature characteristics of samples having the same composition and soaking time but different cooling rates. All the samples show the PTCR behaviour above near 120 °C. The samples prepared at slow cooling rates showed relatively high resistivity. The slope of the PTCR curve ($d\rho/dT$) above the transition temperature and the resistivity jump ($\rho_{max} - \rho_{min}$) increased as the cooling rates decreased. This type of the cooling-rate effect on the resistivity versus temperature characteristics of the samples in this study corresponds to the observations made in the other published studies [19].

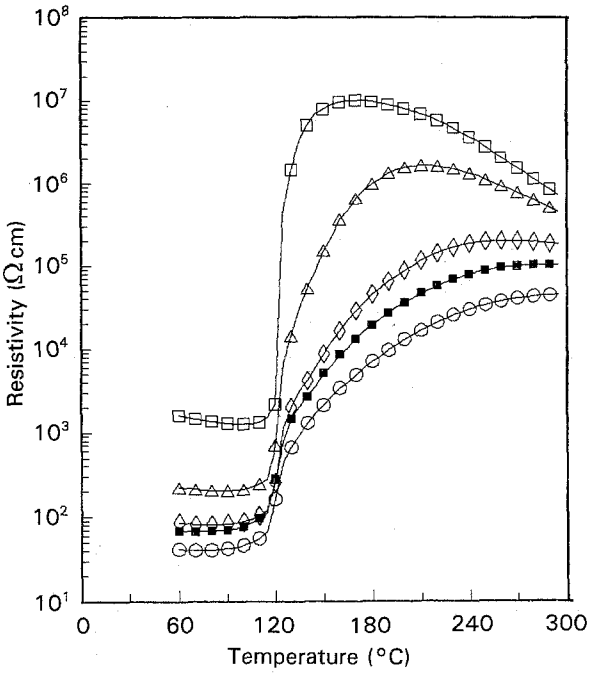

Figure 1 Resistivity versus temperature characteristics of n-type semiconducting $BaTiO_3$ samples having the same composition and soaking time but different cooling rates: (□) 6 °C h^{-1}, (△) 12 °C h^{-1}, (◇) 25 °C h^{-1}, (■) 50 °C h^{-1}, (○) 100 °C h^{-1}.

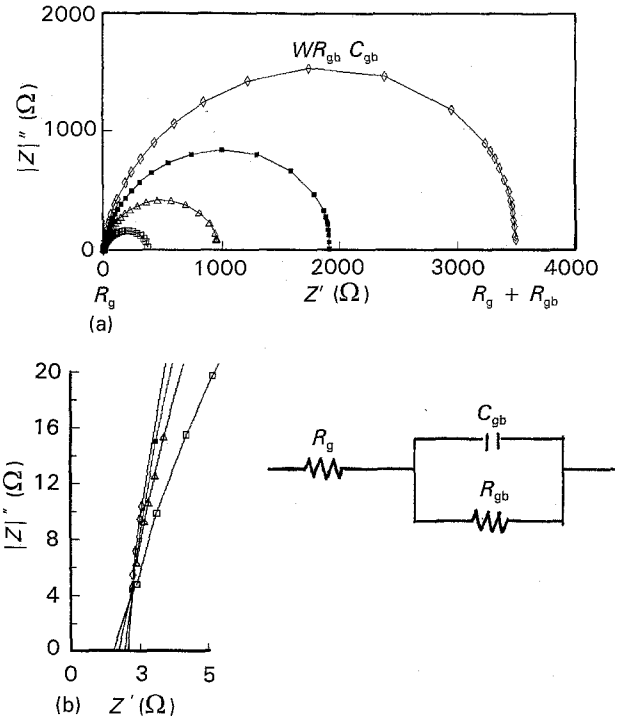

Figure 2 (a) Complex impedance spectra of a sample at different temperatures: (□) 140 °C, (△) 160 °C, (■) 180 °C, (◇) 200 °C. The sample was fabricated with 100 °C h^{-1} cooling rate. (b) The spectra in the high-frequency region and an equivalent circuit representing the spectra.

Fig. 2a shows the complex impedance spectra of the sample (prepared at a cooling rate of 100 °C h^{-1}) at different test temperatures. The impedance spectra of the sample at temperatures lower than 120 °C are not included in the figure, because the values are relatively small compared to the axis range used in the figure.

Within the frequency range of the instrumentation available for this study, a single arc was observed at each test temperature. The size of the arc increased as the test temperature increased, indicating that the temperature increased a particular impedance source in the material responsible for this arc. Fig. 2b shows the spectra in the high-frequency region. The left-hand intersection of the arc did not occur at zero resistance, indicating that the particular impedance source is a serial combination of the grain resistance and the grain-boundary resistance and capacitance as depicted in the figure. Using the equivalent circuit model and $\omega R_{gb}C_{gb} = 1$, where ω is the angular frequency at which the arc representing grain boundary shows minimum reactance, grain resistance can be estimated from the real-axis value at the left-hand intersection of the arc. The grain-boundary resistance and capacitance can be estimated from the real axis value at the right-hand intersection of the arc and the above equation. The grain resistivity and the grain-boundary resistivity data were normalized by N_L and $N_L/2$, respectively, where N_L is the number of the grain-boundary intercepts per unit length of the micrograph. The factor 2 was included because each grain boundary is composed of two depletion layers.

Fig. 3 shows the grain resistivity versus temperature curve for the samples fabricated with different cooling rates. The grain resistivity decreased as the temperature increased up to a certain temperature at which the resistivity increased with the temperature. This observation corresponds to the observation made in another study [20] and indicates that the doped $BaTiO_3$ grain also exhibited relatively weak PTCR behaviour. Heywang [2] claimed that the electrons inside the grain move to the grain-boundary region as the depletion layers were built up near the grain boundary. It may be speculated that the electron concentration across the grain is not uniform but low in the outside region and high in the central region, and, consequently, the grain consists of an electron-depletion region which may cause the weak PTCR behaviour of the grain observed in this study.

Fig. 4 shows the grain-boundary resistivity versus temperature curves for the samples fabricated with different cooling rates. The grain-boundary resistivity decreased as the temperature increased up to a critical temperature at which the resistivity jumps to several orders of magnitude. The grain-boundary resistivity jumps are relatively high compared to the change observed in the grain resistivity versus temperature curves (Fig. 3). Therefore, the observed PTCR behaviour in Fig. 2 is mainly due to the depletion layers formed near the grain boundaries of the donor-doped n-type semiconducting $BaTiO_3$ grains.

Table I shows the room-temperature grain resistivity, the grain-boundary resistivity, the grain-boundary capacitance and the average grain size of the samples fabricated using different cooling rates. The capacitance data in the table were also normalized by $N_L/2$. Both the grain resistivity and the grain-boundary resistivity decreased as the cooling rate increased. The observation made for the cooling-rate effect on the grain-boundary resistivity may be explained using the barium vacancy compensation model in which the slow cooling provided the vacancy with time to diffuse inside the grain, established a relatively high and wide depletion layer and, consequently, caused the sample to have high grain-boundary resistance. According to Heywang's speculation, electrons from the neighbouring grain move to the grain-boundary region as the depletion layers build up near the grain boundary. Therefore, as the depletion layer height and width

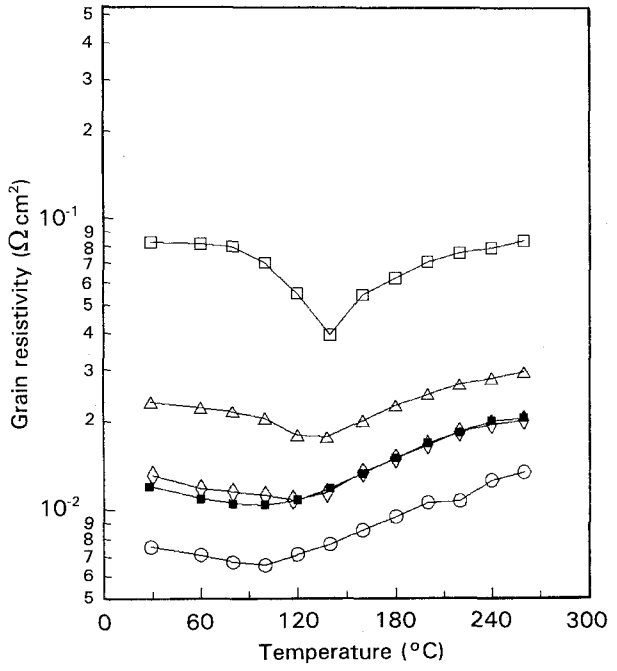

Figure 3 Grain resistivity versus temperature curves for the samples fabricated with different cooling rates: (□) 6 °C h^{-1}, (△) 12 °C h^{-1}, (◇) 25 °C h^{-1}, (■) 50 °C h^{-1}, (○) 100 °C h^{-1}.

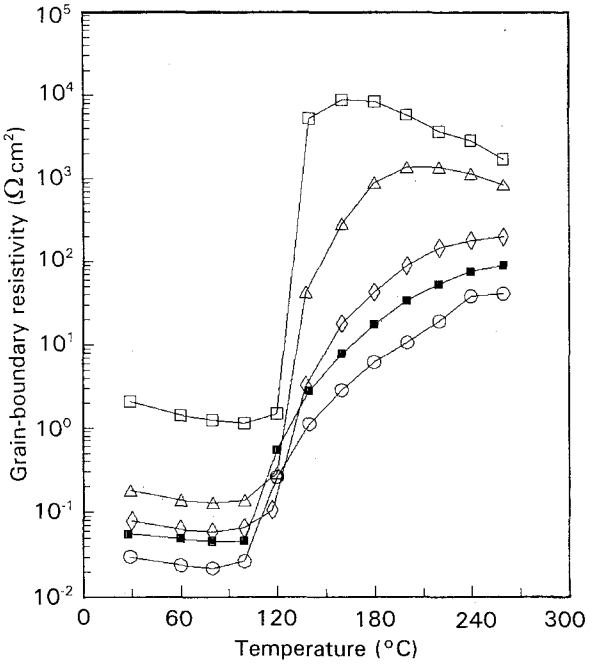

Figure 4 Grain-boundary resistivity versus temperature curves for the samples fabricated with different cooling rates: (□) 6 °C h^{-1}, (△) 12 °C h^{-1}, (◇) 25 °C h^{-1}, (■) 50 °C h^{-1}, (○) 100 °C h^{-1}.

TABLE I Room-temperature complex impedance data of the samples prepared with different cooling rates

Cooling rate (°C h^{-1})	Normalized grain resistivity ($10^{-2}\,\Omega\,cm^2$)	Normalized grain-boundary resistivity ($\Omega\,cm^2$)	Normalized grain-boundary capacitance ($\mu F\,cm^{-2}$)	Grain size (μm)
6	8.24	2.0616	1.17	22.08
12	2.33	0.1803	3.15	21.99
25	1.31	0.0790	4.03	21.20
50	1.20	0.0556	3.97	19.98
100	0.753	0.0304	5.56	18.95

increase, due to the slow cooling rate, the electron concentration decreases, and the grain resistivity increases.

Using the grain-boundary resistivity and the grain-boundary capacitance data in Table I, a straight line was produced in an $\ln\rho$ versus C^{-2} plot at room temperature. The value ρ_0 was estimated from the straight-line interception at the vertical axis of the plot as follows

$$\rho_0 = 1.9526 \times 10^{-2}\,\Omega\,cm^2 \quad (4)$$

The proportionality constant, ρ_0, is not a strong function of temperature. Therefore, one can calculate the values of V_{bi} at other temperatures by substituting Equation 4 into Equation 1 and using the grain-boundary resistivity value at a particular temperature. Fig. 5 shows the calculated built-in potential versus temperature curves for the samples fabricated at different cooling rates. The curves show a shape similar to the resistivity versus temperature curves of the samples (Fig. 1) except that the built-in potential does not decrease at the temperature ranges below the PTCR transition temperature or above the temperature at which maximum resistivity occurred. Slow cooling produced a higher built-in potential.

A donor impurity density, N_D, of the samples used in this study was calculated by 1/40 of the actual Sb_2O_3 doping concentration [21, 22]. Using Equation 3, the width of the depletion layer, W, at each temperature can be estimated. Fig. 6 shows the depletion-layer width versus temperature curves for the samples fabricated with different cooling rates. The depletion-layer width decreased as temperature increased from room temperature to about 80 °C and then showed a rapid increase from above 80 °C, the temperature at which the capacitance rapidly increases in the capacitance versus temperature characteristics of $BaTiO_3$ ferroelectric ceramics. The depletion-layer width did not change after the rapid increase. The sample fabricated at slow cooling rate showed a relatively large depletion-layer width. Because the barium vacancies penetrate deeply inside the grain at slow cooling rates, the depletion-layer width increased as the cooling rate decreased. Because the grain-boundary resistivity of the sample depends on both the built-in potential and the depletion-layer width, it is worthwhile to relate the built-in potential to the depletion-layer width at different temperature. Fig. 7 shows a depletion-layer width versus built-in potential curve for different temperatures of the sample prepared with cooling rate of

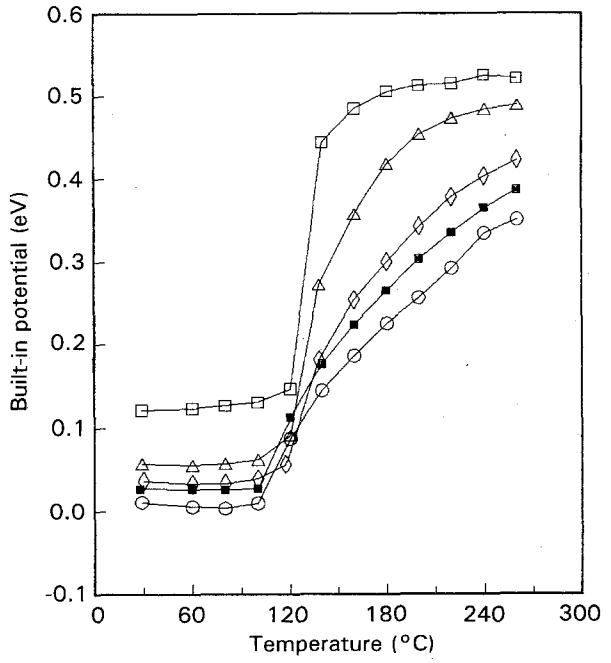

Figure 5 Built-in potential versus temperature curves of the samples fabricated with different cooling rates: (□) 6 °C h^{-1}, (△) 12 °C h^{-1}, (◇) 25 °C h^{-1}, (■) 50 °C h^{-1}, (○) 100 °C h^{-1}.

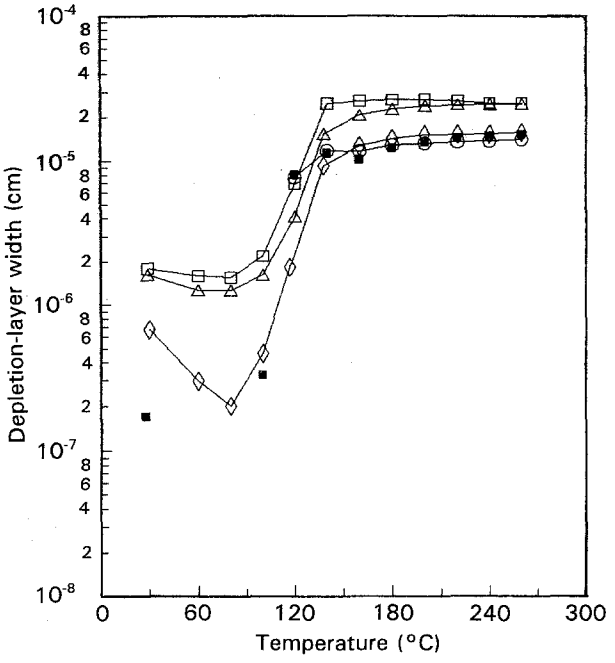

Figure 6 Depletion-layer width versus temperature curves of the samples fabricated with different cooling rates: (□) 6 °C h^{-1}, (△) 12 °C h^{-1}, (◇) 25 °C h^{-1}, (■) 50 °C h^{-1}, (○) 100 °C h^{-1}.

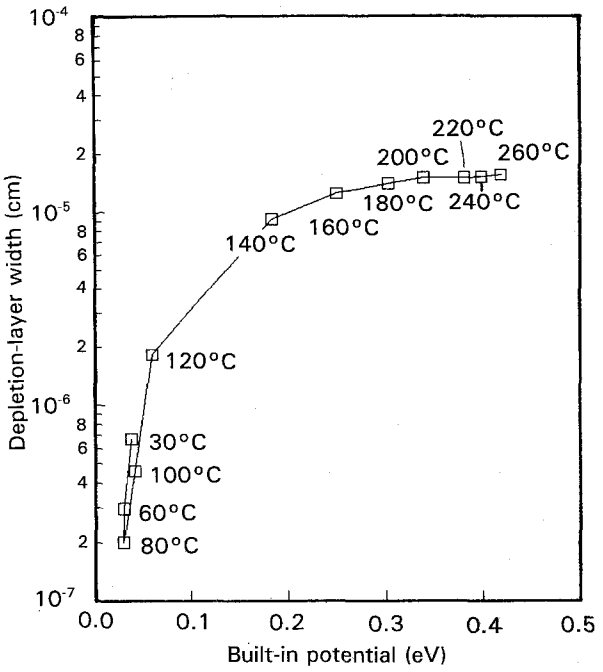

Figure 7 A built-in potential versus depletion-layer width curve at different temperatures for the sample fabricated with 25 °C h^{-1} cooling rate.

25 °C h^{-1}. Each point represents the test temperature. The built-in potential did not change, but the depletion-layer width decreased as the temperature increased up to 80 °C. The grain-boundary resistivity of the sample decreased as the temperature increased in this temperature range, as shown in Fig. 4. Therefore, the observed resistivity decreases in the temperature range is mainly due to the depletion-layer width decrease. After the decrease, both the built-in potential and the depletion-layer width increased as the temperature increased in the temperature range in which the grain-boundary resistivity rapidly increased with temperature, as shown in Fig. 4. As the temperature increased over the range in which both the built-in potential and the depletion-layer width increased, the depletion-layer width did not change but the built-in potential increased. In this temperature range, the grain-boundary resistivity increase rate declined as the temperature increased, as shown in Fig. 4.

4. Conclusions

N-type doped semiconducting $BaTiO_3$ was fabricated at different cooling rates. The cooling-rate effect on the depletion layer of N-type doped $BaTiO_3$ was analysed using d.c. resistivity and a.c. complex impedance spectroscopy. As the cooling rate decreased, the sample resistivity, the slope of the PTCR curve and the resistivity jump increased. These increases were mainly due to the grain-boundary resistivity increase. The grain resistivity also showed relatively weak PTCR behaviour. Slow cooling rates also produced a higher built-in potential and larger depletion-layer width. The grain-resistivity decrease below 80 °C was mainly due to a depletion-layer width decrease. Both the built-in potential and the depletion-layer width showed an increase above 80 °C, which indicates that the observed PTCR behaviour of $BaTiO_3$ was due to the built-in potential and the depletion layer formed near the grain boundary. The rate of increase of the grain-boundary resistance declined as the temperature increased over the transition region.

Acknowledgement

This work was sponsored by Korea Science and Engineering Foundation under contract 911-0606-016-2.

References

1. B. M. KULWICKI, in "Advances in Ceramics", Vol. 1. "Grain Boundary Phenomena in Electronic Ceramics", edited by L. M. Levinson, (American Ceramic Society, Columbus, OH, 1981) pp. 138–54.
2. W. HEYWANG, *Solid-state Electron.* **3** (1961) 51.
3. P. GERTHSEN and K. H. HAERDTL, *Z. Naturforsch. A Astrophys. Phys. Phys. Chem.* **18** (1963) 423.
4. H. IHRG and M. KLERK, *Appl. Phys. Lett.* **35** (1979) 307.
5. W. HEYWANG, *J. Am. Ceram. Soc.* **47** (1964) 484.
6. J. DANIELS and R. WERNICHE, *Philips Res. Rep.* **31** (1976) 544.
7. H. IHRIG and W. PUSCHERT, *J. Appl. Phys.* **48** (1977) 3081.
8. H. BRAUER, *Solid-State Electron.* **17** (1974) 1013, in German.
9. C. A. MILLER, *J. Phys. D Appl. Phys.* **4** (1971) 690.
10. G. GOODMAN, *J. Am. Ceram. Soc.* **46** (1963) 48.
11. G. H. JONKER, *Solid-State Electron.* **7** (1964) 895.
12. J. DANIELS, K. H. HÄRDTE and R. WERNICKE, *Philips Tech. Rev.* **38** (3) (1978/79) 73.
13. S. M. SZE, "Physics of Semiconductor Devices", 2nd Edn. (Wiley, New York, 1981) p. 248.
14. D. Y. WANG and K. UMEYA, *J. Am. Ceram. Soc.* **73** (1990) 669.
15. R. P. BUCK, *Ion-Selective Rev.* **4** (1982) 3.
16. R. N. BASU and H. S. MAITI, to be published.
17. H. S. MAITI and R. N. BASU, *Mater. Res. Bull.* **21** (1986) 1107.
18. FRANK KULCSAR, *J. Am. Ceram. Soc.* **39** (1956) 13.
19. H. S. MAITI and R. N. BASU, in *High Tech. Ceram.*, 38B edited by P. Vincenzinà (Elsevier Science, B.V., 1987) pp. 1883–1892.
20. D. C. SINCLAIR and A. R. WEST, *J. Mater. Sci. Lett.* **7** (1988) 823.
21. J. DANIELS and K. H. HARDTL, *Philips Res. Rep.* **31** (1976) 489.
22. B. G. BRAHMECHA, *Jpn J. Appl. Phys.* **8** (1969) 883.

Received 18 May 1992
and accepted 20 April 1993